FLOW IN GROOVED MICRO-CHANNELS

Alireza Mohammadi
Department of Mechanical and Materials Engineering
The University of Western Ontario
London, Ontario, N6A 5B9, Canada
amoham69@uwo.ca

Jerzy M. Floryan
Department of Mechanical and Materials Engineering
The University of Western Ontario
London, Ontario, N6A 5B9, Canada
mfloryan@eng.uwo.ca

ABSTRACT

Analysis of flows in grooved micro-channels has been carried out. One-dimensional grooves with arbitrary orientation with respect to the channel axis have been considered. It is shown that the drag generation mechanisms can be divided into effects associated (i) with the average position and (ii) with the shapes of the grooves. Three physical mechanisms associated with the shapes have been identified, i.e., re-arrangement of viscous stresses, pressure interaction drag and pressure form drag. Analysis relies on the analytic solutions in the limit of long wavelength corrugation and a novel, grid-less, spectrally-accurate algorithm based on the Immersed Boundary Conditions (IBC) concept for other corrugations.

INTRODUCTION

The need for the re-examination of the role of surface roughness is driven by micro-fluidics applications, where micro- and nano-conduits are expected to have significant surface corrugations (surface roughness) due to the limitations of manufacturing technologies. A number of authors attempted to provide quantitative predictions of pressure losses. Kleinstreuer & Koo (2004) modelled corrugations as layers of porous material. Kandlikar et al. (2005) introduced a set of roughness parameters. Wang (2003) analyzed flow over rectangular grooves/ribs while Thomas et al. (2001) worked with sinusoidal grooves/ribs. These investigations provide phenomenological information about certain classes for roughness forms but do not provide information about the mechanisms of drag generation.

Grooves may lead to flow destabilization and changes in the drag through a bifurcation of the flow field. Centrifugal instability has been identified in the case of Couette (Floryan, 2002) and Poiseuille flows (Floryan, 2003). Floryan and Floryan (2010) studied travelling wave instability, and Szumbarski & Floryan (2006) studied transient growth. Experimental verifications of theoretical predictions dealing with the effects of sinusoidal surface corrugation on the critical Reynolds number have been reported by Asai & Floryan (2006).

The modelling of roughness geometry represents a challenge due to the potentially uncountable number of geometric shapes. This problem has been settled using spectral models of roughness geometry (Floryan, 1997). It has been shown that in many situations it is sufficient to use the leading Fourier mode from the Fourier expansion describing roughness shape to capture the main physical processes (Floryan, 2007). The difficulties associated with solving of the field equations in an irregular flow domain have been settled by using either the immersed boundary conditions method or the domain transformation method (Szumbarski & Floryan, 1999; Husain & Floryan, 2010; Mohammadi & Floryan, 2011). These methods permit determination of flow details with a spectral accuracy for the complete range of roughness shapes being of practical interest.

PROBLEM FORMULATION

Consider flow in a channel bounded by two grooved walls extending to $\pm\infty$ in the x- and z-directions, where the x-axis overlaps with the direction of the flow (Fig.1). The grooves are periodic with wavelengths $\lambda_x=2\pi/\alpha$ and $\lambda_z=2\pi/\beta$, where α and β stand for the wave numbers in the x- and z-directions, respectively. Shapes of the grooves are specified as $y_U(x,z)$ and $y_L(x,z)$, where the subscripts U and L refer to the upper and lower walls, respectively. The grooves are inclined with respect to the flow direction with an angle $\pi/2-\phi$, i.e., the ridges form angle ϕ with the z-axis (see Fig.1). We shall refer to grooves corresponding to $\phi=0°$ as the transverse grooves, $\phi=90°$ as the longitudinal grooves, and $0°<\phi<90°$ as the oblique grooves. The shapes of the grooves can be expressed in terms of Fourier expansions in the form

$$y_U(x,z) = 1 + \sum_{n=-N_A}^{n=N_A} \sum_{m=-N_A}^{m=N_A} H_U^{(n,m)} e^{i(n\alpha x + m\beta z)}, \quad (1a)$$

$$y_L(x,z) = -1 + \sum_{n=-N_A}^{n=N_A} \sum_{m=-N_A}^{m=N_A} H_L^{(n,m)} e^{i(n\alpha x + m\beta z)}, \quad (1b)$$

where $H_U^{(n,m)} = H_U^{(-n,-m)*}$, $H_L^{(n,m)} = H_L^{(-n,-m)*}$, stars denote the complex conjugates, and N_A is the number of Fourier modes needed to describe groove geometry. It is convenient to introduce a different reference system $(\tilde{x},y,\tilde{z})$ where the $\tilde{x}$-axis is perpendicular and the $\tilde{z}$-axis is parallel to the grooves' ridges (see Fig.1). The new system permits description of geometry of the grooves in terms of single Fourier expansions, i.e.,

$$y_U(\tilde{x}) = 1 + \sum_{n=-N_A}^{n=N_A} \tilde{H}_U^{(n)} e^{in\tilde{\alpha}\tilde{x}}, \; y_L(\tilde{x}) = -1 + \sum_{n=-N_A}^{n=N_A} \tilde{H}_L^{(n)} e^{in\tilde{\alpha}\tilde{x}}, \quad (2a,b)$$

where $\tilde{H}_U^{(n)} = \tilde{H}_U^{(-n)*}$, $\tilde{H}_L^{(n)} = \tilde{H}_L^{(-n)*}$ and $\tilde{\alpha}$ stands for the wave number in the $\tilde{x}$-direction. Transformation between the (x,y,z) and $(\tilde{x},y,\tilde{z})$ systems has the form

$$\tilde{x} = \cos(\phi)x - \sin(\phi)z, \; \tilde{z} = \sin(\phi)x + \cos(\phi)z. \quad (3a,b)$$

Relations between coefficients of expansions (1) and (2) have the form

$$H_U^{(n,m)} = \tilde{H}_U^{(n)} \text{ for } n = -m, \; H_U^{(n,m)} = 0 \text{ for } n \neq -m, \quad (4a,b)$$

$$\hat{H}_L^{(n,m)} = H_L^{(n)} \text{ for } n = -m, \; \hat{H}_L^{(n,m)} = 0 \text{ for } n \neq -m, \quad (5a,b)$$

and relations between the wave numbers take the form

$$\alpha = \tilde{\alpha}\cos(\phi), \; \beta = \tilde{\alpha}\sin(\phi). \quad (6a,b)$$

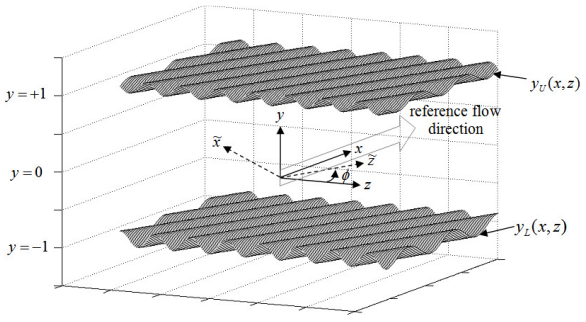

Figure 1. Channel with grooved walls. The (x,y,z) coordinate system is flow-oriented and the $(\tilde{x},y,\tilde{z})$ system is grooved-oriented. The angle ϕ shows the relative orientation of both systems.

Flow between smooth walls is taken as the reference flow and the direction of this flow defines the reference flow direction. This flow is driven by a constant pressure gradient directed in the negative x-direction resulting in the velocity and pressure fields which in the auxiliary reference system take the form

$$\tilde{\mathbf{V}}_0(y) = [\tilde{u}_0, \tilde{v}_0, \tilde{w}_0] = [(1-y^2)\cos(\phi), 0, (1-y^2)\sin(\phi)], \quad (7)$$

$$\tilde{p}_0(\tilde{x},\tilde{z}) = -2Re^{-1}[\tilde{x}\cos(\phi) + \tilde{z}\sin(\phi)] + c, \quad (8)$$

where $\tilde{\mathbf{V}}_0$ is the reference velocity vector, $\tilde{p}_0$ is the reference pressure and c denotes an arbitrary constant. It is advantageous to carry out numerical solution using the $(\tilde{x},y,\tilde{z})$-system defined by Eq.(3). The total velocity and pressure fields can be expressed in this system as

$$\tilde{\mathbf{V}}(\tilde{\mathbf{x}}) = [\tilde{u}_0(y) + \tilde{u}_1(\tilde{x},y), \tilde{v}_1(\tilde{x},y), \tilde{w}_0(y) + \tilde{w}_1(\tilde{x},y)], \quad (9)$$

$$\tilde{p}(\tilde{\mathbf{x}}) = \tilde{p}_0(\tilde{x},\tilde{z}) + \tilde{p}_1(\tilde{x},y,\tilde{z}) = \tilde{p}_0(\tilde{x},\tilde{z}) + h_{\tilde{x}}\tilde{x} + h_{\tilde{z}}\tilde{z} + \tilde{q}(\tilde{x},y), \quad (10)$$

where subscripts 0 and 1 refer to the reference flow and flow modifications due to the presence of the grooves, respectively, $h_{\tilde{x}}$ and $h_{\tilde{z}}$ denote modifications of the mean pressure gradient in the $\tilde{x}$- and $\tilde{z}$-directions, respectively and $\tilde{q}(\tilde{x},y)$ describes the $\tilde{x}$-periodic part of the pressure modification.

The flow in the auxiliary reference system is a function of only two coordinates, i.e., $(\tilde{x},y)$, which reduces the field equations to the following form

$$\partial_{\tilde{x}}\tilde{u}_1 + \partial_y\tilde{v}_1 = 0, \quad (11)$$

$$\tilde{u}_1\partial_{\tilde{x}}\tilde{u}_1 + \tilde{v}_1\partial_y\tilde{u}_1 + \tilde{v}_1 D\tilde{u}_0 + \tilde{u}_0\partial_{\tilde{x}}\tilde{u}_1 = -h_{\tilde{x}} - \partial_{\tilde{x}}\tilde{q} + Re^{-1}\nabla^2\tilde{u}_1, \quad (12)$$

$$\tilde{u}_1\partial_{\tilde{x}}\tilde{v}_1 + \tilde{v}_1\partial_y\tilde{v}_1 + \tilde{u}_0\partial_{\tilde{x}}\tilde{v}_1 = -\partial_y\tilde{q} + Re^{-1}\nabla^2\tilde{v}_1, \quad (13)$$

$$\tilde{u}_1\partial_{\tilde{x}}\tilde{w}_1 + \tilde{v}_1\partial_{\tilde{y}}\tilde{w}_1 + \tilde{v}_1 D\tilde{w}_0 + \tilde{u}_0\partial_{\tilde{x}}\tilde{w}_1 = -h_{\tilde{z}} + Re^{-1}\nabla^2\tilde{w}_1, \quad (14)$$

where $\nabla^2 = \partial^2/\partial\tilde{x}^2 + \partial^2/\partial y^2$ and $D = d/dy$. The reader may note that equations (11)–(13) do not contain $\tilde{w}_1$ and thus they form an independent system that can be solved separately from (14). It can be shown that such separation may be carried out only for certain types of flow constraints.

In order to form a close system of equations one needs to specify two arbitrary closing conditions. Four types of conditions/constraints are of interest: fixed volume flow rate per unit width in the x-direction, fixed volume flow rate per unit width in the z-direction, fixed mean pressure gradient in the x-direction and fixed mean pressure gradient in the z-direction.

The boundary conditions take the form

$$\tilde{u}_1(y_U(\tilde{x})) = -\tilde{u}_0(y_U(\tilde{x})), \; \tilde{v}_1(y_U(\tilde{x})) = 0, \; \tilde{w}_1(y_U(\tilde{x})) = -\tilde{w}_0(y_U(\tilde{x})), \quad (15a\text{-}c)$$

$$\tilde{u}_1(y_L(\tilde{x})) = -\tilde{u}_0(y_L(\tilde{x})), \; \tilde{v}_1(y_L(\tilde{x})) = 0, \; \tilde{w}_1(y_L(\tilde{x})) = -\tilde{w}_0(y_L(\tilde{x})). \quad (16a\text{-}c)$$

Only when either the volume flow rate constraints or the pressure gradient constraints are chosen, Eqs.(11)–(13) with boundary conditions (15a,b) and (16a,b) become independent of w_1 and can be solved separately. Their solution describes a

two-dimensional motion in the ($\tilde{x}$,y) plane. The flow in the $\tilde{z}$-direction can be determined in the second step of the solution process by solving equation (14) with the boundary conditions (15c) and (16c). If the flow rate and the pressure gradient constraints are mixed, the decoupling does not occur and one needs to solve Eqs. (11)–(14) as a single system.

NUMERICAL METHOD

The above problems were solved using spectral discretization method based on the Fourier expansions in the $\tilde{x}$- and $\tilde{z}$- directions and Chebyshev expansions in the y-direction. The problem of irregularity of the solution domain in the y-direction has been overcome by the use of the Immersed Boundary Conditions (IBC) method (Szumarski and Floryan, 1999). This method relies on the use of a fixed computational domain extending in the y-direction far enough so that it completely encloses the grooved channel (see Fig.1) and imposition of flow boundary conditions is carried out through specially constructed boundary relations.

The solution process consists of two steps, i.e., solution of the nonlinear problem (11-13) to determine flow in the ($\tilde{x}$,y) plane and the follow up solution of the linear problem (14) to determine flow in the (y,$\tilde{z}$) plane. The former problem is solved using an iterative technique described by Mohammadi and Floryan (2011). Efficient solution methods for the latter problem are discussed by Mohammadi and Floryan (2011). Results presented in this paper are based on transverse grooves (ϕ=0) with fixed flow rate constraint.

DISCUSSION OF RESULTS

Pressure gradient h_x induced by the grooves can be expressed in terms of friction factor and this method of presentation will be used in this presentation.

Pressure loss in a channel can be expressed as

$$\Delta p^* / \Delta L^* = \left(2\partial p / \partial x\right)\left(\rho^* U_s^2\right)/(2L_s)\,, \tag{17}$$

where stars denote dimensional quantities, L_s and U_s are the length and velocity scales, respectively, Δp^* stands for the pressure loss over the channel length ΔL^* and ρ^* denotes the density. The typical length scales L_s are either half of the channel opening L or the hydraulic diameter D_h=4A/P, where A is the cross-sectional area and P is the wetted perimeter of the cross-section; D_h=4L for a plane channel with opening 2L. The typical velocity scales U_s are either the maximum of the reference velocity U_{max} or the average reference velocity U_{ave}=2/3 U_{max}. The friction factor f is defined by

$$f = -2\partial p / \partial x \tag{18}$$

and it takes different numerical values depending on the length and velocity scales. There are four possible combinations: Scale A is based on L_s=L and U_s=U_{max}, Scale B is based on L_s=L and U_s=U_{ave}, Scale C is based on L_s=D_h and U_s=U_{max}, and Scale D is based on L_s=D_h and U_s=U_{ave}. The pressure gradient and its corresponding friction factors written in scale D for the channel with transverse grooves takes the form

$$\partial p / \partial x = \partial p_0 / \partial x + h_x\,, \tag{19}$$

$$f_x = -2\partial p_0 / \partial x - 2h_x = f_{0x} + f_{1x}\,, \tag{20}$$

where $\partial p_0/\partial x$=–48/Re_D is the pressure gradient of the reference flow, Re_D=$U_{ave}D_h/\nu$, f_x denotes the total friction factor in the x-direction, f_{0x} denotes the reference friction factor (i.e., friction factor for the smooth channel), and f_{1x} refers to the modification of the friction factor in the x-direction. All results of friction factors will be presented using scale D from above, i.e.,

$$f_{x,D} * Re_D = 96 - 48 * h_x * Re\,,\ f_{0x,D} * Re_D = 96\,, \tag{21a,b}$$

$$f_{1x,D} * Re_D = -48 * h_x * Re\,. \tag{21c}$$

Grooves may produce changes in the flow through two separate mechanisms, i.e., (i) change in the average channel opening and (ii) through spatial modulations induced by the shape of the grooves. Since the former effect may be introduced inadvertently when creating grooves, it is necessary to account for it properly when interpreting results. We shall start discussion with the former effect.

Effect of the average position of the grooves

Consider a channel with two flat walls located at y_U=1 and y_L=–1+ε. Maintenance of the same flow rate as in the reference channel (Q=4/3) requires imposition of a pressure gradient of the magnitude

$$\partial p / \partial x = -2Re^{-1}(1-\varepsilon/2)^{-3}\,. \tag{22}$$

The change of pressure gradient h_x generated by the change in the channel opening can be easily evaluated as

$$h_x = \partial p_1 / \partial x = \partial p / \partial x - \partial p_0 / \partial x = 2Re^{-1}\left[1-(1-\varepsilon/2)^{-3}\right] \tag{23}$$

and expressed in terms of the friction factor as

$$f_{1x,D} * Re_D = -48 * h_x * Re = -96\left[1-(1-\varepsilon/2)^{-3}\right]. \tag{24}$$

We shall now modify the above channel by adding sinusoidal transverse grooves (ϕ=0°) to the lower wall. The channel geometry is described in the (x,y,z) and ($\tilde{x}$,y,$\tilde{z}$) coordinate systems as

$$y_U = 1\,,\ y_L(x) = -1 + S_{ave} + (S/2)\cdot\cos(\alpha x)\,, \tag{25a,b}$$

$$y_L(\tilde{x}) = -1 + S_{ave} + (S/2)\cdot\cos(\tilde{\alpha}\tilde{x})\,, \tag{25c}$$

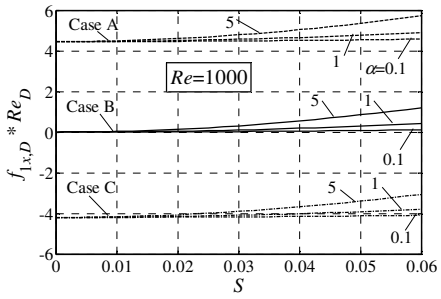

Figure 2. Variations of the modification friction factor $f_{1x,D}$*Re_D as a function of the grooves' amplitude S for representative values of the grooves' wave number α for the flow Reynolds numbers Re=1000. Shape of the walls is given by Eq.(26) with S_{ave}=0.03, 0, –0.03 in Cases A, B, C, respectively.

where S, S_{ave} and $\tilde{\alpha}$ (=α) define the height, the average position and the wave number of the grooves. Variations of the additional pressure loss (expressed in term of the modification friction factor) as a function of the groove amplitude S are illustrated in Fig.2 for three average positions S_{ave} for selected values of the groove wave numbers α and the flow Reynolds number Re. Cases A, B and C correspond to S_{ave} = 0.03, 0 and –0.03, respectively. When S = 0 all cases correspond to a smooth channel, where the effect of the grooves' shape is absent but the effect of change in the average channel opening remains. Equation (24) gives additional friction factors for smooth channel in all these cases as

$$\text{Case A: } f_{1x,D} * Re_D = 4.45 \text{ ,Case B: } f_{1x,D} * Re_D = 0 \text{ ,}$$
$$\text{Case C: } f_{1x,D} * Re_D = -4.19 \text{ .} \qquad (26)$$

Results for Case B are obvious, and friction factors for Cases A and C are shifted by constants 4.45 and –4.19, respectively. Addition of grooves, i.e., increase of S, results in an increase of the friction factor in all cases considered. The reader may note, however, that the curves for cases A, B and C shown in Fig.2 are shifted by the amounts given by Eq.(26) in the whole range of S considered. This demonstrates that the effect of the average position of the wall on the pressure losses can be separated from the effect of shape of the grooves; change in the average wall position is accounted for by an additive constant that can be predicted analytically and added to the computed pressure loss associated with the shape of the grooves. It is sufficient therefore to concentrate in the rest of this analysis of the effects of shape of the grooves only.

Effect of the dominant geometric/flow parameters

Consider transverse sinusoidal grooves placed at the lower wall, i.e.,

$$y_U = 1 \text{ , } y_L(x) = -1 + (S/2) \cdot \cos(\alpha x) \text{ .} \qquad (27)$$

Figure 3 shows the variations of the modification friction factor $f_{1x,D}$*Re_D as functions of different dominant geometric/flow parameters. These results show that the modification friction factor $f_{1x,D}$*Re_D increases with increase in any of grooves' wave number α, grooves' amplitude S or the flow Reynolds number Re.

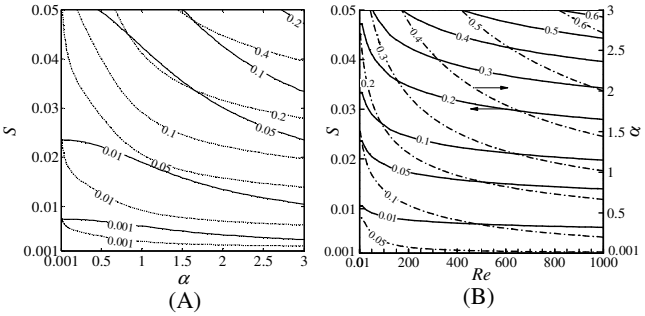

Figure 3. Variations of the modification friction factor $f_{1x,D}$*Re_D as functions of different parameters for transverse grooves with shape defined by Eq.(27). Fig.3A– $f_{1x,D}$*Re_D as functions of grooves' wave number α and grooves' amplitude S for two values of the flow Reynolds number Re=0.01 (solid lines) and Re=1000 (dash lines), Fig.3B– $f_{1x,D}$*Re_D as functions of the flow Reynolds number Re and grooves' amplitude S (solid lines) for grooves with α=3 and as functions of the flow Reynolds number Re and grooves' wave number α (dash-dot lines) for grooves with S=0.05.

Long wavelength grooves

Consider a grooved channel with geometry described by Eq.(27). In the limit $\alpha \to 0$ solution can be assumed in the form of expansions

$$u = u_0 + \alpha u_1 + 0(\alpha^2) \text{ , } v = v_0 + \alpha v_1 + 0(\alpha^2) \text{ ,}$$
$$p = \alpha^{-1} p_{-1} + p_0 + 0(\alpha) \text{ .} \qquad (28a\text{-}c)$$

Substitution of above expansions into the governing equations, application of transformation in the form

$$\xi = \alpha x \text{ , } \eta = (y-1)[1 - S\cos(\alpha x)/4]^{-1} + 1 \text{ ,} \qquad (29a,b)$$

retention of terms of the two leading orders of magnitude and solution of the resulting equations lead to

$$u_0 = M \ [f(\xi)]^{-1}(1-\eta^2) \text{ ,} \qquad (30a)$$

$$u_1 = 0.25 Re M^2 S \sin(\xi)[f(\xi)]^{-1}\left(-\frac{1}{30}\eta^6 + \frac{1}{6}\eta^4 - \frac{11}{70}\eta^2 + \frac{5}{210}\right), \qquad (30b)$$

$$v_0 = 0 \text{ , } v_1 = 0.25 MS \sin(\xi)[f(\xi)]^{-1}(-\eta^3 + \eta^2 + \eta - 1) \text{ ,} \qquad (31a,b)$$

$$\frac{dp_{-1}}{d\xi} = -H[f(\xi)]^{-3} \text{ , } \frac{dp_0}{d\xi} = \frac{6}{35} M^2 S \sin(\xi)[f(\xi)]^{-3} \text{ ,} \qquad (32a,b)$$

$$p_{-1} = -H\left(2+S^2/16\right)\left(1-S^2/16\right)^{-5/2}\arctan\left[\left(1+S/4\right)^{1/2}\left(1-S/4\right)^{-1/2}\tan\left(\xi/2\right)\right]$$
$$+0.125HS\sin(\xi)\left[0.75S\cos(\xi)+S^2/16-4\right]\left(1-S^2/16\right)^{-2}\left[f(\xi)\right]^{-2}, \quad (33a)$$
$$p_0 = (12/35)M^2\left\{-\left[f(\xi)\right]^{-2}+\left(1-S/4\right)^{-2}\right\}, \quad (33b)$$

where pressure has been normalized to have p=0 at ξ=0. In the above, M=1+3Q_{1x}/4 and $M=\left(1-Reh_x/2\right)\left[1-\left(S/4\right)^2\right]^{5/2}\left[1+\left(S/4\right)^2/2\right]^{-1}$ for the fixed flow rate and the fixed mean pressure gradient constraints, respectively, Q_{1x} is the modification of flow rate due to the presence of the grooves for the case of mean pressure gradient constraint, $f(\xi)=\left[1-S\cos(\xi)/4\right]$ and H=2M/Re. Results displayed in Fig.2 for the y-velocity component demonstrate that the range of validity of Eqs. (30)-(33) extends up to α=0(1) if Re is small (Re=0.1); at Re=1000 this range decreases to α=0(10^{-2}).

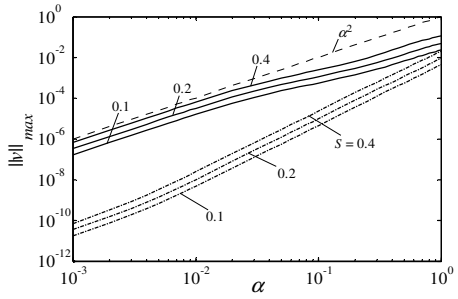

Figure 4. Variations of the difference $\|v\|_{max} = \sup_{-\pi\le\xi\le\pi,\,-1\le\eta\le1}\left|v_a(\xi,\eta)-v_c(\xi,\eta)\right|$ between the asymptotic v_a and the complete v_c solutions for the y-velocity component as a function of the corrugation wave number α for selected values of the corrugation amplitude S and for the flow Reynolds numbers Re=1000 (solid lines) and Re=0.1 (dash-dot lines) for the fixed mass flow rate constraint (Q_{1x}=0).

The drag is generated solely by viscous shear in the case of smooth walls. Presence of the corrugation alters distribution of shear and this leads to changes in the shear drag. Corrugation represents an obstacle to the flow and this leads to generation of the pressure drag.

Distribution of the x-component of shear and the total viscous force acting on the fluid at the lower wall have the forms

$$dF_{x,visc} = -2MRe^{-1}\left[f(\xi)\right]^{-2}+\alpha\frac{4}{105}M^2S\sin(\xi)\left[f(\xi)\right]^{-2}+0(\alpha^2), \quad (34a)$$
$$F_{x,visc} = -4\alpha^{-1}MRe^{-1}\pi\left[1-(S/4)^2\right]^{-3/2}+0(\alpha). \quad (34b)$$

Distribution of the x-component of the pressure force acting on the fluid at the lower wall has the form

$$dF_{x,\,pres} = 0.5S\left[p_{-1}+\alpha p_0+0(\alpha^2)\right]\sin(\xi). \quad (35)$$

The total pressure force can be evaluated through numerical integration of Eq.(35). It is instructive, however, to replace $dp_{-1}/d\xi$ in Eq.(32a) with its Fourier expansion and integrate this expansion with respect to ξ to arrive at a more convenient analytical expression for the pressure, i.e.,

$$p_{-1} = -H\left[1+(S/4)^2/2\right]\left[1-(S/4)^2\right]^{-5/2}\xi$$
$$-(3/4)HS\left[1-(S/4)^2\right]^{-5/2}\sin(\xi)+\cdots \quad (36)$$

Integration of Eq.(35) over one corrugation period, say from γ to γ+2π, with p_{-1} expressed by Eq.(36) shows that terms omitted in Eq.(36) as well as p_0 do not contribute to the total force. The total force has the form

$$F_{x,pres} = F_{x,form}+F_{x,inter} = \left\{\alpha^{-1}SH\pi\left[1+(S/4)^2/2\right]\left[1-(S/4)^2\right]^{-5/2}\right\}\cos(\gamma)$$
$$-\alpha^{-1}(3/8)S^2H\pi\left[1-(S/4)^2\right]^{-5/2}+0(\alpha), \quad (37)$$

where the first term is associated with the mean pressure gradient acting on an obstacle (corrugation) and thus we shall refer to it as the "form drag". The form drag is a periodic function of γ with the amplitude defined by the curly bracket. These variations of the form drag need to be accounted for in interpretation of any experimental measurements as in the case of a corrugation in the form of a depression the form drag will likely reduce the total drag while in the case of the corrugation in the form of a bump the form drag will likely increase the total drag.

The second term in (37) arises out of an interaction of the periodic part of p_{-1} with the wall geometry and thus we shall refer to it as the "interaction drag". The part of the pressure field that gives rise to the "interaction drag" is proportional to sin(ξ) (see Eq.36) while the corrugation shape is described by cos(ξ); π/2 shift between both distributions results in the interaction drag. The interaction drag does not depend on the location of the test segment of the corrugation, i.e., does not depend on γ.

It can be shown that the distribution of the x-component of the local viscous forces $dG_{x,visc}$ as well as the total viscous force $G_{x,visc}$ at the upper wall are same as at the lower wall, i.e., $dG_{x,visc}$=$dF_{x,visc}$, $G_{x,visc}$=$F_{x,visc}$. Pressure does not generate any forces in the x-direction at the upper wall.

Balance of forces acting on a control volume extending over one wavelength and corresponding to γ=–π gives the total pressure force F_{total} acting between the left and right control surface as

$$F_{total} = \alpha^{-1}\frac{8\pi}{Re}+\left\{\alpha^{-1}\frac{8\pi}{Re}\left[1+(S/4)^2/2\right]\left[1-(S/4)^2\right]^{-5/2}\left(1+S/4\right)-\alpha^{-1}\frac{8\pi}{Re}\right\}, \quad (38)$$

where the second term on the RHS describes change in the force due to the presence of the corrugation. This force is opposed by the shear force F_s, by the force F_{form} due to the form drag and by the force F_{inter} due to the interaction drag, which have forms

$$F_s = \alpha^{-1} 8\pi Re^{-1} + \alpha^{-1} 8\pi Re^{-1} \left\{ \left[1 - (S/4)^2 \right]^{-3/2} - 1 \right\}, \quad (39)$$

$$F_{form} = \alpha^{-1} 2S\pi \, Re^{-1} \left[1 + (S/4)^2/2 \right] \left[1 - (S/4)^2 \right]^{-5/2}, \quad (40)$$

$$F_{inter} = \alpha^{-1} 0.75 S^2 \pi Re^{-1} \left[1 - (S/4)^2 \right]^{-5/2}. \quad (41)$$

Results displayed in Fig.5 demonstrate that the total drag increases rapidly with an increase of the corrugation amplitude. The largest part of this increase comes from the form drag, followed by the interaction drag, and the smallest comes from the re-arrangement of the viscous drag. Contributions of the pressure form and interaction drag increase to the level of 35% and 23% of the total force, respectively, when corrugation amplitude reaches value S=2. The form drag, the interaction drag and the additional viscous drag are responsible for 45%, 30% and 25% of this increase.

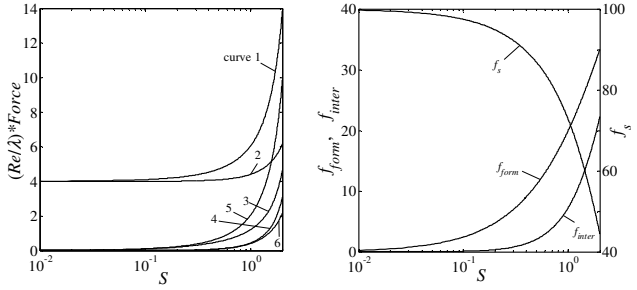

Figure 5. Variations of the total force per unit channel length $(Re/\lambda)*F_{total}$ and its various components (Fig.5A; see Eqs (38-41)) and percentage of these contributions (Fig.5B) as a function of the corrugation amplitude S. In the above, $\lambda=2\pi/\alpha$ denotes the wavelength of the channel, curves 1, 2, 3, 4, 5, 6 correspond to $(Re/\lambda)*F_{total}$, $(Re/\lambda)*F_s$, $(Re/\lambda)*F_{form}$, $(Re/\lambda)*F_{inter}$, $(Re/\lambda)*F_{total,1}$ and $(Re/\lambda)*F_{s,1}$, respectively, $F_{total,1}$ and $F_{s,1}$ denote the difference between the total forces and viscous forces in the corrugated and smooth channels, respectively. Fractions describing contributions of the form, interaction and viscous drag are defined as $f_{form}=(F_{form}/F_{total})*100$, $f_{inter}=(F_{inter}/F_{total})*100$ and $f_s=(F_s/F_{total})*100$, respectively.

CONCLUSIONS

Flows through channels with grooved walls have been analyzed using a combination of analytical solutions and numerical simulations based on the novel, grid-less, spectral algorithm implementing the Immersed Boundary Conditions concept. It has been shown that surface grooves may produce changes in the flow through two separate mechanisms, i.e., (i) change in the average channel opening and (ii) through spatial modulations induced by the shape of the grooves. Three mechanisms for generation of additional pressure losses have been identified in the later case. The first one is associated with the alteration of the shear stress distribution at the smooth and corrugated walls, the second one is associated with the presence of an obstacle (corrugation) in a flow with a mean pressure gradient and is referred to as the form drag, and the third one is associated with the interaction of the periodic part of the pressure field and the surface geometry and occurs due to a phase shift between them.

REFERENCES

Asai, M., and Floryan, J. M., 2006, "Experiments on the Linear Instability of Flow in a Wavy Channel", *European Journal of Mechanics B/Fluids*, Vol. 25, pp. 971-986.

Floryan, J. M., 1997, "Stability of Wall Bounded Shear Layers with Simulated Distributed Surface Roughness", *Journal of Fluid Mechanics*, Vol. 335, pp. 29-55.

Floryan, J. M., 2002, "Centrifugal Instability of Couette Flow over a Wavy Wall", *Physics of Fluids*, Vol. 14, pp. 312-322.

Floryan, J. M., 2003, "Vortex Instability in a Converging-Diverging Channel", *Journal of Fluid Mechanics*, Vol. 482, pp. 17-50.

Floryan, J. M., 2007, "Three-Dimensional Instabilities of Laminar Flow in a Rough Channel and the Concept of Hydraulically Smooth Wall", *Euroupean Journal of Mechanics B/Fluids*, Vol. 26, pp. 305-329.

Floryan, J. M., and Floryan, C., 2010, "Traveling Wave Instability in a Diverging-Converging Channel", *Fluid Dynamics Research*, Vol. 42, 025509, pp. 1-20.

Husain, S. Z., and Floryan, J. M., 2010, "Spectrally-Accurate Algorithm for Moving Boundary Problems for the Navier-Stokes Equations", *Journal of Computational Physics*, Vol. 229, pp. 2287-2313.

Kandlikar, S. G., Schmitt, D., Carrano, A. L., and Taylor, J. B., 2005, "Characterization of Surface Roughness Effects on Pressure Drop in Single-Phase Flow in Mini-Channels", *Physics of Fluids*, Vol. 17, 100606, pp. 1-11.

Kleinstreuer, C., and Koo, J., 2004, "Computational Analysis of Wall Roughness Effects for Liquid Flow in Micro-Conduits", *Journal of Fluids Engineering*, Vol. 126, pp. 1-9.

Mohammadi, A., and Floryan, J. M., 2011, "Spectral Algorithm for Analysis of Flows in Grooved Channels", to appear in the *International Journal for Numerical Methods in Fluids* (accepted Feb15.2011).

Szumarski, J., and Floryan, J. M., 1999, "A Direct Spectral Method for Determination of Flows over Corrugated Boundaries", *Journal of Computational Physhics*, Vol. 153, pp. 378-402.

Szumbarski J., and Floryan, J. M., 2006, "Transient Disturbance Growth in a Corrugated Channel", *Journal of Fluid Mechanics*, Vol. 568, pp. 243-272.

Thomas, S. C., Lykins, R. C., and Yerkes, K. L., 2001, "Fully-Developed Laminar Flow in Sinusoidal Grooves", *Journal of Fluids Engineering*, Vol. 123, pp. 656-661.

Wang, C. Y., 2003, "Flow over a Surface with Parallel Grooves", *Physics of Fluids*, Vol. 15, pp. 1114-1121.